JCTC Journal of Chemical Theory and Computation

Double-Metal-Ion/Single-Metal-Ion Mechanisms of the Cleavage Reaction of Ribozymes: First-Principles Molecular Dynamics Simulations of a Fully Hydrated Model System

Mauro Boero,*[,†] Masaru Tateno,[‡,||] Kiyoyuki Terakura,[§,||] and Atsushi Oshiyama[†]

Institute of Physics, University of Tsukuba, 1-1-1 Tennodai, Tsukuba, Ibaraki 305-8571, Japan, Center for Biological Resources and Informatics, Tokyo Institute of Technology, Nagatsuta 4259, Midori-ku, Yokohama 226-8501, Japan, Division of Frontier Research, Creative Research Initiative "Sousei", Hokkaido University, Kita 21, Nishi 10, Kita-ku, Sapporo 001-0021, Japan, and Research Institute for Computational Sciences, National Institute of Advanced Industrial Science and Technology, 1-1-1 Umezono, Tsukuba, Ibaraki 305-8568, Japan

Received March 14, 2005

Abstract: The role of metal cations (Mg^{2+}) in the cleavage reaction of fully hydrated RNA enzymes is investigated via Car−Parrinello calculations. We find that the action of two metal catalysts is the most efficient way to promote, on one hand, the proton abstraction from $O^{2'}-H$ that triggers the nucleophilic attack and, on the other hand, the weakening and subsequent cleavage of the $P-O^{5'}$ bond. The elimination of one of the two metal cations is shown to lead to an increase in the activation energy. Furthermore, we also find that an OH^- included in the coordination shell of the Mg^{2+} close to $O^{2'}$ promotes the initial proton abstraction and prevents its transfer to the ribozyme in both single- and double-metal-ion pathways, consistently with the experiment. This suggests that in real ribozyme systems, the double-metal-ion reaction mechanism in the presence of an OH^- anion is favored with respect to single-metal-ion mechanisms.

1. Introduction

The great importance of catalytic RNA molecules (ribozymes) stems from their ability to cleave other target RNA molecules with a high specificity and, hence, to inhibit gene expression.[1−18] The hydrolysis of the phosphodiester proceeds by cleaving the $P-O^{5'}$ bonds of a RNA target molecule at a specific site,[1,2] a reaction known as transesterification, giving as a product 2′,3′-cyclic phosphate and a departing 5′-hydroxyl group.[8−14] The reaction path of the transesterification has been discussed by several authors over the years.[1−20] For the ongoing discussion, we shall refer to the generally accepted scheme, reported in Figure 1, shared by all the self-cleaving ribozymes;[1,14] namely, the reactant (1) overcomes an activation barrier passing across the trigonal bipyramidal (TBP) transition state, carrying a pentacoordinated P, (2) before sliding down to the final product (3).[1,2] Two metal cations, indicated in Figure 1 as M_1 and M_2, are expected to act as catalysts, since a large variety of RNA enzymes are known to be metalloenzymes.[19−30] The most common metal used in experiments is Mg^{2+}. However, several divalent metal ions have been used either in vivo or in vitro,[21−27] and the transesterification rate has been shown to depend also on the nature of the metal catalyst adopted.[22−28]

A lot of effort, from both experimentalists[1−28] and theoreticians,[29−43] has been devoted to unraveling the intimate

* To whom correspondence should be addressed. Tel.: +81-29-8535921, e-mail: boero@comas.frsc.tsukuba.ac.jp.
† University of Tsukuba.
‡ Tokyo Institute of Technology.
§ Hokkaido University.
|| National Institute of Advanced Industrial Science and Technology.

10.1021/ct050066q CCC: $30.25
Published on Web 07/07/2005

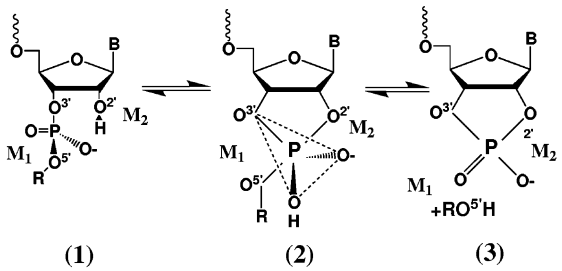

Figure 1. Schematic cleavage reaction path for a general transesterification reaction promoted by two divalent metal ions M_1 and M_2.

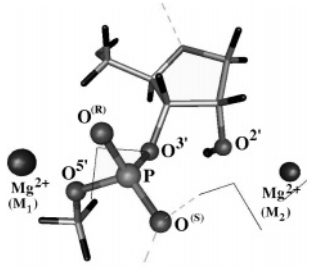

Figure 2. Average configuration of the RNA system used in the simulations. All the most relevant atoms are labeled according to the standard notations and displayed as balls; the metal ions are also indicated as M_1 and M_2 in parentheses for the sake of clarity. Thick sticks show the rest of the structure, with the H atoms in black and the C atoms in gray. Thinner v-shaped sticks are some of the surrounding water molecules, and dashed lines indicate the H bonds.

details of the transesterification reaction. Yet, because of the intrinsic complexity of the mechanism, several questions are still unanswered and many details of the reaction pathway still escape direct experimental probes. Nevertheless, past experimental and theoretical studies suggest that the important elementary processes on which one must focus can be summarized in (i) the role of divalent metal cations as a Lewis acid[27] and the number of ions involved in the reaction, (ii) the deprotonation of $O^{2'}-H$,[43−48] (iii) the nucleophilic attack of $O^{2'}$ to P, (iv) $P-O^{5'}$ bond cleavage, and (v) pseudorotations of the phosphodiester.

The aim of the present work is to analyze the effects of the actors, such as metal cations, water, and OH^-, on the above elementary processes. We can remark, however, that, as the present study does not deal with the system in acidic conditions, pseudorotation is not expected to be an important issue.[1] We focus on two fundamental issues: the nature of the interactions of the RNA moiety with the divalent metal cations and the proton abstraction from the $O^{2'}-H$ group, along with its subsequent transfer either to the ribozyme departing group or to the solvent. We give microscopic insight into these two issues via first-principles molecular dynamics for both a single-metal-ion and a double-metal-ion mechanism, computing and comparing activation barriers and reaction pathways for the various cases, evidencing how two metal catalysts are both important in lowering the overall energy barrier and in promoting the reaction. Simulations in which either M_1 or M_2 is removed show that an energetically more demanding reaction path arises: on one hand, the absence of M_2 makes the proton abstraction from the $O^{2'}-H$ group, and the related nucleophilic attack, more problematic; on the other hand, if M_1 is absent, a larger activation barrier exists for the cleavage of the $P-O^{5'}$ bond, indicating that the partial electron withdrawal from the $P-O^{5'}$ bond operated by M_1 plays a special role in the enhancement of the reaction. It is shown that the unoccupied 3s orbitals of Mg^{2+} withdraw electrons from the chemical bonds of the nearby RNA system, thus weakening them and favoring the above-mentioned two reactions, that is, proton abstraction from $O^{2'}-H$ and cleavage of the $P-O^{5'}$ bond. Since an OH^- is often postulated to be involved in the catalytic reactions of metalloenzymes, we analyze the effects induced by the presence of an OH^- hydroxyl anion in the solvation shell of M_2, both in the single-ion and in the double-ion reaction mechanisms. We find that, besides its noticeable effect in triggering the initial proton abstraction, it is an essential ingredient to explain, for example, the absence of proton transfer in the reaction.[44]

2. Computational Methods

First-principles molecular dynamics simulations were performed within the Car−Parrinello[49,50] (CP) scheme in the framework of Kohn−Sham (KS) density functional theory (DFT),[51] including gradient corrections on the exchange and correlation functional after Hamprecht, Cohen, Tozer, and Handy (HCTH).[52] This particular choice of the exchange correlation has already been assessed and turns out to be comparable to a B3LYP hybrid functional[52,53] in reproducing geometries, energetics, and hydrogen-bonding properties.[31,40,53] Whenever open-shell calculations are required, spin polarization within the same HCTH framework was taken into account, and valence-core interactions are described by Troullier−Martins[54] norm-conserving pseudopotentials. In the case of Mg, nonlinear core corrections[55] were included with cutoff radii of 1.104 and 1.343 Å for the s and p angular moments, respectively, and a core density cutoff radius of 0.762 Å, and valence electrons are represented in a plane wave basis set with an energy cutoff of 70 Ry. This cutoff value has already been shown to be necessary to get a basis set convergence sufficiently accurate to describe the fast oscillations of the O wave functions in the vicinity of the core region and to get structural and energetic parameters comparable to all-electron approaches within the same functional.[40−42,53] The simulated systems consist of (*N*, *V*, *T*) ensembles containing one RNA anion moiety including one ribose unit, as shown in Figure 2, amounting to 26 atoms, plus 60 water molecules and two metal cations or 61 H_2O molecules plus a single Mg^{2+} for the double- and single-metal-ion cases, respectively. The pristine pure water system was per-equilibrated alone at standard density (1.0 g/cm^3) and temperature (300 K) in a cubic supercell of side $L =$ 13.146 Å with periodic boundary conditions for about 6 ps. Then, a space suitable to allocate the solute ribozyme model was cleaved as described in ref 31. The temperature was set to 300 K and controlled via a Nosé−Hoover thermostat chain.[56−58] An integration step of 4.0 au (0.0967 fs) with a fictitious electron mass of 600 au ensured good control of the conserved quantities.

The reaction path was sampled via the metadynamics approach,[59,60] by adding to the CP Lagrangean L^{CP} the harmonic degrees of freedom of the collective variables s_α plus the history-dependent Gaussian potential $V(s_\alpha,t)$

$$L = L^{CP} + \sum_\alpha 1/2 M_\alpha \dot{s}_\alpha{}^2 - \sum_\alpha 1/2 k_\alpha [s_\alpha(q) - s_\alpha]^2 - V(s_\alpha,t) \quad (1)$$

where the argument q of $s_\alpha(q)$ can be any function of an arbitrary set of atomic coordinates, electronic wave functions, and so forth. In our cases, we use collective variables that account for the formation of the bond between P and $O^{2'}$, the cleavage of the $P-O^{5'}$ bond, and any other variable involved in the reaction that is expected to be slow with respect to the ps time scale of ordinary first-principles molecular dynamics. Specific details about the set of s_α adopted will be given for each case to support the discussion. In each simulation, a new Gaussian contribution is added to the potential $V(s_\alpha,t)$ every $\Delta t = 0.012$ ps, amounting to 150 molecular-dynamics-generated configurations, as explained in ref 60. By monitoring the running averages

$$\langle \phi^k \rangle_t = \frac{1}{t} \int_0^{t \le \Delta t} \phi^k(t')\, dt' \quad (2)$$

where the integrands $\phi^\kappa(t')$ ($k = 1, 2, 3$) are $E^{KS} = \phi^1$ (the KS total energy), $K_e = \phi^2$ (the electronic fictitious kinetic energy), and $T_{ion} = \phi^3$ (the ionic temperature), we checked that these quantities are sufficiently well-equilibrated during the short sampling time Δt and preserve the adiabaticity of the CP dynamics. This allows for an accurate exploration of the free energy surface (FES) without requiring a too heavy computational workload. The free energy landscape $F(s_\alpha)$ results as

$$F(s_\alpha) = -\lim_{t\to\infty} V(s_\alpha,t) + \text{const.} \quad (3)$$

where the limit has to be intended in the sense given in ref 60; that is, additional Gaussians are added until the selected portion of the phase space, spanned by the collective variables, is saturated. The history-dependent potential has the explicit form

$$V(s_\alpha,t) = \int_0^t dt' |\dot{\vec{s}}(t')| \delta\left\{ \frac{\dot{\vec{s}}(t')}{|\dot{\vec{s}}(t')|} [\vec{s} - \vec{s}(t')] \right\} A(t') \exp\left\{ -\frac{[\vec{s} - \vec{s}(t')]^2}{2(\Delta s)^2} \right\} \quad (4)$$

where $\vec{s} = (s_1, ..., s_\alpha, ...)$ and the Gaussian amplitude $A(t')$, having the dimensions of an energy, is sampled in the interval (0.02, 0.4) kcal/mol. Computing free energies is, anyhow, always a very delicate issue. In this work, in an attempt at estimating free energy differences, we simply inspect the overall free energy landscape given by eq 3 and seek for the minimum energy barrier on $V(s_\alpha)$ in an interval $\Omega = [s_1{}^a, s_1{}^b] \times [s_2{}^a, s_2{}^b] \times ...$ around the transition value of each collective variable, separating the reactants from the products, that is

$$V(s_a{}^{TS}) = \min_{\{s_\alpha \in \Omega\}} [V(s_\alpha)] \quad (5)$$

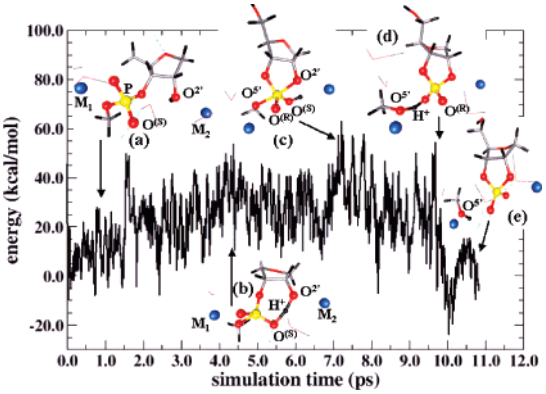

Figure 3. Potential energy during the metadynamics simulation at 300 K. The main steps are (a) the initial configuration, (b) the proton transfer from $O^{2'}-H$, (c) the TBP transition structure, (d) the final proton transfer to the departing group, and (e) the final state. The arrows indicate approximately the location of the different configurations along the metadynamics trajectory, and the initial configuration is assumed as a reference point on the energy axis. The most relevant atoms are labeled in the snapshots according to Figure 2, and the colors adopted are black for H atoms, gray for C, red for O, yellow for P, and blue for Mg^{2+}.

and assuming, in each case, as a reference level, the initial stable local minimum $V(s_\alpha{}^0)$ at $s_\alpha(t = 0) = s_\alpha{}^0$, that is, before any Gaussian penalty potential is added. The latter corresponds to the initial free dynamics of the system equilibrated on the reactants side. We then use $\Delta F = V(s_\alpha{}^{TS}) - V(s_\alpha{}^0)$. Of course, this estimation is biased by how well-resolved the sampled free energy hypersurface is. The dispersions reported in the following paragraphs refer, instead, to the dynamical averages, at a given $s_\alpha(t)$ over the aforementioned 150 CP steps performed before updating $s_\alpha(t)$, that is, $\delta(\Delta F)^2 = \langle V^2(s_\alpha)\rangle - [V(s_\alpha)]^2$. As for the total energy, we simply time-averaged over the trajectory intervals at fixed $V(s_\alpha)$, that is, in between a Gaussian contribution and the subsequent one, along the evolution of the system as displayed in Figures 3 and 7. Further details will be given in the following paragraphs whenever needed to support the discussion.

In some cases, the activation barrier was also checked via thermodynamic integration within the Blue Moon ensemble method,[61] assuming as a reaction coordinate the distance $P-O^{2'}$. In doing so, equilibration times of ~2.0 ps for each sampled constraint ensured meaningful statistics and a good convergence of the running averages of both the constraint force and the KS total energy. Total and free energies are affected by an average error bar typical of first-principles approaches and amounting to 2−3 kcal/mol. Mulliken charges are computed by a standard projection of the KS states onto atomic orbitals.[62]

3. Results and Discussion

Before starting simulations using phase space sampling techniques (either metadynamics or the Blue Moon ensemble method) to analyze the reaction path leading to the transesterification,[1,2] we pre-equilibrated, for about 8 ps via standard unconstrained CP[49,50] molecular dynamics at room temper-

Table 1. Main Geometrical Parameters of the Initial Configurations and TBP Structures as Obtained during the Dynamical Simulations Described in the Text[a]

initial	no metal	one Mg^{2+} close to $O^{5'}$	one Mg^{2+} close to $O^{2'}$	two Mg^{2+}	one Mg^{2+} with OH^-	two Mg^{2+} with OH^-
$P-O^{2'}$	4.134 ± 0.141	3.901 ± 0.135	3.924 ± 0.128	4.202 ± 0.262	3.904 ± 0.095	3.970 ± 0.114
$P-O^{5'}$	1.621 ± 0.050	1.646 ± 0.059	1.630 ± 0.055	1.649 ± 0.064	1.637 ± 0.066	1.662 ± 0.072
$M_1-O^{5'}$		2.156 ± 0.159		2.279 ± 0.107		2.510 ± 0.185
$M_1-O^{(R)}$		2.072 ± 0.122		2.157 ± 0.119		2.052 ± 0.139
$M_2-O^{2'}$			2.188 ± 0.068	2.277 ± 0.106	2.051 ± 0.152	2.598 ± 0.389
$O^{2'}PO^{5'}$	$97.6 \pm 10.1°$	$105.4 \pm 4.9°$	$112.0° \pm 8.6°$	$99.1° \pm 6.7°$	$115.1° \pm 7.9°$	$94.6° \pm 7.2°$
TBP	no metal	one Mg^{2+} close to $O^{5'}$	one Mg^{2+} close to $O^{2'}$	two Mg^{2+}	one Mg^{2+} with OH^-	two Mg^{2+} with OH^-
$P-O^{2'}$	1.689 ± 0.051	1.760 ± 0.063	1.783 ± 0.099	1.809 ± 0.107	1.809 ± 0.098	1.812 ± 0.097
$P-O^{5'}$	1.667 ± 0.067	1.781 ± 0.119	1.805 ± 0.138	1.820 ± 0.137	1.795 ± 0.097	1.821 ± 0.105
$M_1-O^{5'}$		2.170 ± 0.204	3.052 ± 0.489[a]	2.190 ± 0.149		2.212 ± 0.142
$M_1-O^{(R)}$		2.104 ± 0.258		2.089 ± 0.228		2.131 ± 0.232
$M_2-O^{2'}$			3.504 ± 0.590	2.401 ± 0.233	2.018 ± 0.160	3.235 ± 0.365
$O^{2'}PO^{5'}$	$178.1 \pm 6.7°$	$177.0 \pm 7.8°$	172.3 ± 13.9	$179.4 \pm 5.9°$	$178.4° \pm 5.1°$	$178.9° \pm 5.3°$

[a] The value is the $M_2-O^{5'}$ distance since a large distortion, shown in Figure 6, brings M_2 close to $O^{5'}$.

ature $T = 300$ K,[56−58] the RNA model structure in a neutral solution with two Mg^{2+} metal cations in the vicinity of $O^{2'}$ and $O^{5'}$. As expected, the average equilibrium structure (Figure 2) shows that the two metal ions occupy stable positions close to the phosphate; more precisely, the Mg^{2+} corresponding to M_1 includes in its solvation shell the $O^{5'}$ atom, whereas $O^{2'}$ participates with the solvation shell of M_2. The main geometrical parameters of the initial equilibrated structures used in our simulations are reported in Table 1, along with the TBP states, and hereafter, we shall refer to them whenever necessary to support the discussion.

3.1. Double-Metal-Ion Mechanism in the Absence of OH^- Hydroxyl Anion. The reaction path was sampled assuming, as a starting point, this equilibrated configuration and using the metadynamics[59,60] approach. In this case, as inferred from the accepted reaction mechanism and the known experimental evidence,[1,2] the collective variables were chosen to be the coordination number between P and $O^{2'}$ [$s_1(t) = N_{coord}(P-O^{2'})$], the coordination number between P and $O^{5'}$ [$s_2(t) = N_{coord}(P-O^{5'})$], and the coordination number between $O^{2'}$ and its initially bound H atom [$s_3(t) = N_{coord}(O^{2'}-H)$]. Here and in the following, we adopt the definition of N_{coord} introduced in refs 60 and 63, that is, the B coordination around A

$$N_{coord}(A-B) = \frac{1}{N_A}\sum_{I=1}^{N_A}\sum_{J=1}^{N_B}\frac{1-(r_{IJ}/d_{AB})^6}{1-(r_{IJ}/d_{AB})^{12}} \qquad (6)$$

where N_A and N_B are the number of atoms of species A and B, respectively, r_{IJ} is the interatomic distance, and d_{AB} is the typical equilibrium distance or chemical bond between A and B. The fictitious effective masses in the Lagrangean of eq 1 were set to $M_1 = M_2 = 30$ au and $M_3 = 50$ au, and the harmonic coupling constants were $k_1 = k_2 = 0.6$ au and $k_3 = 0.8$ au. The result of the simulation is summarized in Figures 3 and 4. Namely, in a neutral environment, the starting structure (Figure 3a) undergoes, first, a deprotonation of the $-O^{2'}-H$ (Figure 3b) with the transfer of the proton from $O^{2'}$ to the $O^{(S)}$ oxygen, and not to *pro-R* oxygen $O^{(R)}$ (Figure 3c). During the dynamics, the system equilibrates with the *pro-R* oxygen being coordinated to the metal ion M_1 and sharing the solvation shell of this Mg^{2+} with $O^{5'}$, as inferred from experiments[43,44]. $O^{2'}$, in turn, comes close to $O^{(S)}$, and both of them coordinate to M_2. An intramolecular hydrogen bond (H bond) $-O^{2'}-H\cdots O^{(S)}$ is then formed, leading to the proton transfer. This is shown in Figure 4 by the variable s_3—the coordination number of $O^{2'}$—that, during the simulation, jumps between 0 and 1 from 3.4 to 6.2 ps[64] as long as the proton is shared between $O^{2'}$ and $O^{(S)}$. The average configuration is shown in snapshot b in Figure 3. Eventually, when the new $P-O^{2'}$ bond is formed, at about $t = 6.2$ ps, s_1 stabilizes to values around 1 and s_3 decreases to zero. This moment of the simulation represents the nucleophilic attack, leading to the formation of a monoanionic/monoprotic TBP intermediate[2] shown in snapshot c of Figure 3, and the energy barrier for the proton transfer amounts to $\Delta E = 8.1 \pm 1.9$ kcal/mol and $\Delta F = 6.9 \pm 1.6$ kcal/mol for the total and free energies, respectively. In this case, a minimum local barrier was found at $s_3 = 0.48$, whereas $s_1 = 0.55$ (i.e., $P-O^{2'}$ bond not yet formed) and $s_2 = 0.80$ (i.e.,

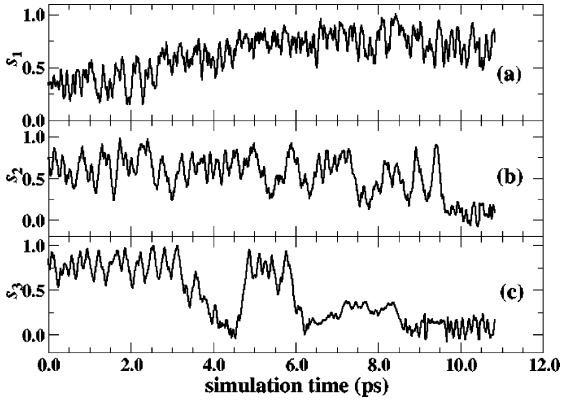

Figure 4. Collective variables as a function of the metadynamics simulation time; s_1, s_2, and s_3 are the coordination numbers of (a) P with $O^{2'}$, (b) P with $O^{5'}$, and (c) $O^{2'}$ with its initially bound H. Further details are given in the text.

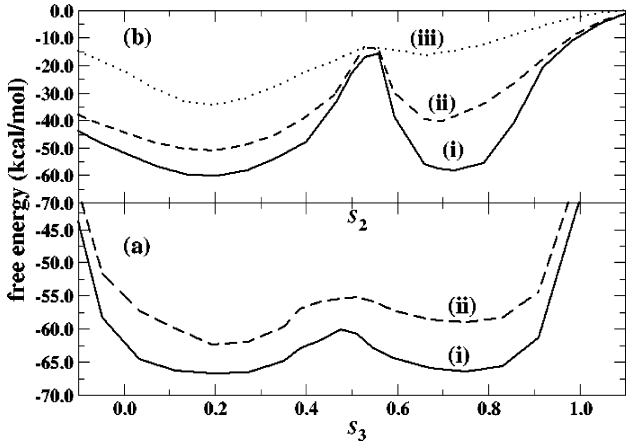

Figure 5. Reconstructed free energy landscape according to eq 4. In panel a, $V(s_1,s_2,s_3)$ is shown as a function of s_3 at (s_1, s_2) = (0.55, 0.80), solid curve (i), and at (s_1, s_2) = (0.65, 0.70), dashed curve (ii), to evidence the $O^{2'}$ deprotonation activation energy. In panel b, $V(s_1,s_2,s_3)$ is shown as a function of s_2 at fixed (s_1, s_3) = (0.80, 0.10), (0.75, 0.15), and (0.70, 0.20) in i (solid curve), ii (dashed curve), and iii (dotted curve), respectively, relevant to the $P-O^{5'}$ bond cleavage.

$P-O^{5'}$ bond not yet broken). This is represented by curve i in panel a of Figure 5 and corresponds roughly to the average configuration (b) of Figure 3. In the same panel, a nearby slice is also reported (dashed curve), representing the free energy profile along the same s_3 collective variable for (s_1, s_2) = (0.65, 0.70) to show how the free energy landscape evolves by moving on the $V(s_\alpha)$ hypersurface in proximity of this transition state.

The system then continues its exploration of the FES until $O^{5'}$ and $O^{2'}$ reach the two axial positions[1] (Table 1), and the $P-O^{5'}$ bond is cleaved before a pseudorotation can occur. Once this bond is cleaved, the departing $R-O^{5'}$ (R, in the present model, being CH_3) group migrates away together with the solvation shell of M_1, to which $O^{5'}$ belongs, and $O^{(R)}$ is no longer coordinated to M_1 (Figure 3e). Since we controlled the coordination number $N_{coord}(O^{2'}-H)$, we see, of course, a drop in its value to zero when the deprotonation occurs (Figure 4).

After the cleavage of the $P-O^{5'}$ bond, the strengthened $P-O^{(S)}$ bond leads to the destabilization of the $O^{(S)}-H$ bond and the proton is released and donated to the $R-O^{5'}$ group that reverts to $R-O^{5'}-H$ (Figure 3d and e). No transfer of the proton to the *pro-R* oxygen was found, since it is hindered by the relatively large distance separating $O^{(R)}$ from H^+. On the other hand, the direct transfer of a proton to the departing group, mediated in our case by $O^{(S)}$, is not totally unexpected and may indeed occur, for example, in the presence of NH_4^+.[43]

By repeating the simulation twice, we noticed that another viable possibility exists. Namely, after the $P-O^{5'}$ bond breaking, the H^+ transferred to the *pro-S* oxygen is spontaneously donated to a nearby H-bound H_2O molecule that, in turn, becomes an OH_3^+, and eventually, the proton is dispersed in the solvent. The departing group forms an H-bonded $R-O^{5'}\cdots H_2O$ complex with another nearby water molecule and eventually gives rise, spontaneously, to the reaction $R-O^{5'} + H_2O \rightarrow R-O^{5'}-H + OH^-$.[65]

Table 2. Computed Activation Barriers (kcal/mol)[a]

	no metal	one Mg^{2+}	two Mg^{2+}	one Mg^{2+} with OH^-	two Mg^{2+} with OH^-
ΔE	60.1 ± 3.1	55.2 ± 2.8[b] 57.3 ± 2.7[c]	46.5 ± 3.0	51.6 ± 2.9[c]	43.8 ± 2.5
ΔF	58.5 ± 2.4	54.0 ± 2.5[b] 55.5 ± 2.5[c]	44.7 ± 2.3	49.2 ± 2.7[c]	41.9 ± 2.2

[a] The error bars reported here are computed as mean square dispersions of the free and total energies during the dynamical sampling of the stationary points. [b] One Mg^{2+} close to $O^{5'}$. [c] One Mg^{2+} close to $O^{2'}$.

The lowest activation barrier for the $P-O^{5'}$ cleavage reaction was identified on the free energy hypersurface at (s_1, s_2, s_3) = (0.80, 0.55, 0.10), as shown in Figure 5b, and this amounts to $\Delta E = 46.5 \pm 3.0$ kcal/mol and $\Delta F = 44.7 \pm 2.3$ kcal/mol for the total and free energies, respectively (Table 2), either in the case in which the released H^+ coming from $O^{(S)}-H$ is transferred to the departing $R-O^{5'}$ group or in the case in which the proton is dispersed in the solvent. In both cases, the collective variables are the same and the final proton transfer is found to be a barrierless process. We remark that the small entropic contribution, in this case, can be ascribed to several causes, namely, the uncertainty affecting the energy barrier estimates due to both the definition adopted and the finite resolution in the free energy reconstruction, the error bars affecting both the total and the free energy, and the fact that, at the transition state, the newly formed $P-O^{2'}$ bond, leading to a pentacoordinated P atom, along with a stabilization of the solvation shells of the two metal ions, makes the system slightly more rigid, thus reducing the entropic contribution that, indeed, is larger by about a factor of two for the initial or final local minima.

A simulation on this same system was performed within the Blue Moon ensemble theory,[61] assuming as a reaction coordinate the distance $P-O^{2'}$. Although the reaction path turned out similar to that of the metadynamics case, as far as the cleavage and proton transfer are concerned, the estimated activation energies turned out to be higher by ~2.0 kcal/mol with respect to the metadynamics estimations. As discussed in ref 63, this seems to be due to the insufficiency of a single reaction coordinate in controlling all the *slow* degrees of freedom involved in the reaction. These activation energies are lower (by about 10 kcal/mol) than analogous barriers computed on this same system in the absence of any metal catalyst (Table 2).[31] Indeed, when metal catalysts are not around, the proton abstraction from $-O^{2'}-H$ occurs simultaneously with the nucleophilic attack and results in a bond switching of $O^{2'}$ from H to P. This is accompanied by several breakings and formations of H bonds with the water molecules of the solvent that contribute to the rising activation barrier. On the other hand, as an inspection of the electronic structure and Mulliken population analysis has evidenced (Table 3), a positive metal ion at the M_2 site withdraws electrons from the $O^{2'}$ oxygen, belonging to its solvation shell, thus weakening the $O^{2'}-H$ bond and favoring the proton release. In an analogous way, the Mg^{2+} located in the vicinity of $O^{5'}$ weakens the $P-O^{5'}$ bond by displacing the electron distribution toward its positive center of charge, thus favoring the cleavage reaction.

Table 3. Mulliken Atomic Charges on the Most Important Atoms in the Initial Configurations and in the Transition States in the Presence of Two Mg^{2+} Metal Cations[a]

atom	initial state	TBP
P	+1.921	+1.786
$H^{2'}$	+0.381	+0.257
$O^{2'}$	−0.389	−0.330
$O^{3'}$	−0.472	−0.355
$O^{5'}$	−0.381	−0.294
M_1	+1.567	+1.442
M_2	+1.558	+1.470

[a] The atom labeling is the same as that in Figure 1.

The electronic structures of the initial (average) configuration and of the TBP transition state were analyzed in terms of Mulliken population,[62] reported in Table 3 for the most relevant atoms involved. As it can be noticed, on one hand, in the initial stage, when the proton abstraction from $O^{2'}-H$ is expected to occur, $O^{2'}$ has a Mulliken charge lower than that of $O^{3'}$ and comparable to that of $O^{5'}$. Indeed, $O^{2'}$ and $O^{5'}$ are part of the solvation shell of M_2 and M_1, respectively. On the other hand, in the TBP configuration, whose main geometrical parameters are listed in Table 1, the Mulliken charges on top of $O^{3'}$ and $O^{5'}$ decrease if compared to the initial state, as a result of the $P-O^{2'}$ bond formation. In particular, the small Mulliken charge of $O^{5'}$ may imply an easier cleavage of $P-O^{5'}$ with respect to a pseudorotation. Let us note also that the presence of the solvent, leading to the H-bonds' formation, alters significantly the Mulliken charges of the O atoms with respect to the vacuum case reported in Table 2 of ref 31. We can infer that spatially extended empty s orbitals, contributed by divalent cations, become partially occupied by withdrawing electrons from those O atoms of the phosphate that belong to the solvation shell of the metal cation. In fact, by analyzing the electronic states of the starting average configuration (Figure 3a) and of the intermediate TBP structure (Figure 3c), we noticed that the spread of the LUMO + 1 orbital,[66] corresponding to the 3s unoccupied states of the metal cations M_1, overlaps $O^{5'}$. As a word of warning, we must acknowledge that,as a result of the energy gap underestimation inherent in these DFT approaches, the location of LUMO + 1 on the energy axis might be lower than in reality and closer to the valence band, thus leading to an overestimation of its interaction with the occupied states. Hence, the picture given above should be intended more as a qualitative trend rather than a precise quantitative estimation.

3.2. Single-Metal-Ion Mechanism in the Absence of OH^- Hydroxyl Anion. A question that remains still unanswered is how many metal ions we really need to enhance the reaction efficiently.[1,30] In an attempt at addressing this issue, we performed two other auxiliary metadynamics simulations by replacing, alternatively, M_1 and M_2 with a water molecule. By separately eliminating the first and the second Mg^{2+}, it is possible to analyze, in detail, the effect of the two metal cations. In our first simulation, we eliminated M_2 from the initial structure of Figure 2 by replacing it with a H_2O molecule and, keeping all the simulation parameters unaltered, we performed a metadynamics run identical to that of the previous case. Contrary to the case in which two metal ions are present, here, the proton abstraction from $-O^{2'}-H$ did not occur until the system reached the TBP structure (Table 1) and occurred in a way similar to the case with an absence of metal ions.[31] The formation of the TBP transition state occurs for a $P-O^{2'}$ bond length of 1.715 Å, shorter than the corresponding TBP formed in the presence of M_2 ($P-O^{2'} = 1.741$ Å), and the release of the proton occurs simultaneously. In fact, only when $O^{2'}$ approaches P, forming a new chemical bond, does the oxygen $O^{2'}$ become over-coordinated (3-fold) and the proton is released. But this is in contrast with the accepted mechanism[1,2] that describes the nucleophilic attack as a consequence of the deprotonation[45,46] of the $O^{2'}-H$ group, which, in this scheme, should precede and not follow the formation of the $P-O^{2'}$ bond. As a consequence, the energy barrier, estimated as described in the previous paragraphs, increases to $\Delta E = 55.2 \pm 2.8$ kcal/mol and $\Delta F = 54.0 \pm 2.5$ kcal/mol. We remark, in passing, that this mechanism seems to be inconsistent with the experiments.[44] The Mg^{2+} located at the M_1 site occupies a dynamically stable catalytic site and does not seem to participate in this first stage of the reaction. Instead, it helps in weakening the $P-O^{5'}$ bond in a way very similar to what was described in the former paragraph and promotes the bond cleavage. Since this bond cleavage is expected to be the rate-limiting step of the reaction, the metal M_1 contributes to the lowering, by about 5 kcal/mol, of the overall energy barrier compared to the case of no metal catalyst. The remaining difference is mostly due to geometrical distortions (see Table 1) and H bonds breaking and forming with the H_2O molecules filling the space formerly occupied by M_2.

On the other hand, when the Mg^{2+} at the M_1 site was eliminated, the deprotonation of $-O^{2'}-H$ was still promoted by the metal cation M_2. However, the proton release occurs close to the transition state and the breaking of the $P-O^{5'}$ bond turns out to be more problematic. In fact, the TBP undergoes a *spontaneous* distortion (Figure 6a and Table 1) that brings both $O^{5'}$ and $O^{2'}$ in the solvation shell of M_2. In these conditions, the proton of $-O^{2'}-H$ is directly transferred to $O^{5'}$ (Figure 6b) and the only available Mg^{2+} also participates in the breaking of the $P-O^{5'}$ bond (Figure 6c). The overall activation energies read $\Delta E = 57.3 \pm 2.7$ kcal/mol and $\Delta F = 55.5 \pm 2.5$ kcal/mol (Table 2); hence, they are not too different with respect to the previous single-metal case. This clearly indicates that the system has a natural tendency to search for available metal cations in order to make the reaction proceed along the smoothest possible path. However, we must remark that the distortion that our model system undergoes in these conditions might well be due to the relatively high mobility of the small $-O^{5'}-CH_3$ group. In a real ribozyme system, such a distortion could be hindered by the more bulky $-O^{5'}-R$, and this suggests that a double-metal-ion mechanism might be favored with respect to a single-metal one. Work is now underway to clarify this point using the whole (hydrated) ribozyme experimental structure.

3.3. The Role of an OH^- Hydroxyl Anion: Double-Metal-Ion Mechanism. In the general reaction of metalloenzymes,[47,48] an OH^- is often postulated to be present in

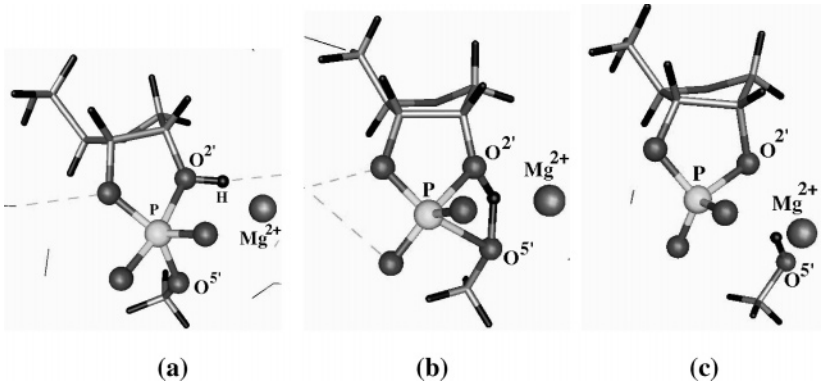

Figure 6. Snapshots of the main steps of the reaction in the presence of a single Mg^{2+} close to $O^{2'}$. The principal atoms are shown as balls and labeled. Color code and graphical representations are the same as those of the preceding figures.

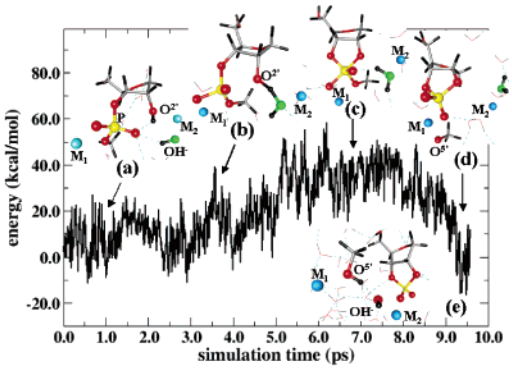

Figure 7. Potential energy for the case of the OH^- hydroxyl anion. The main steps are (a) the initial configuration, (b) the proton abstraction from $O^{2'}-H$, (c) the TBP transition structure, (d) the final $P-O^{5'}$ bond cleavage, and (e) the final product in which a water molecule undergoes a spontaneous dissociation, donating a proton to the departing $O^{5'}$ group. The arrows indicate approximately the location of the various configurations along the metadynamics trajectory, and the initial configuration is assumed as a reference point on the energy axis. Main atoms are labeled and shown as balls; the colors are the same as those of Figure 3, apart from the O belonging to the original OH^- shown in green for the sake of clarity.

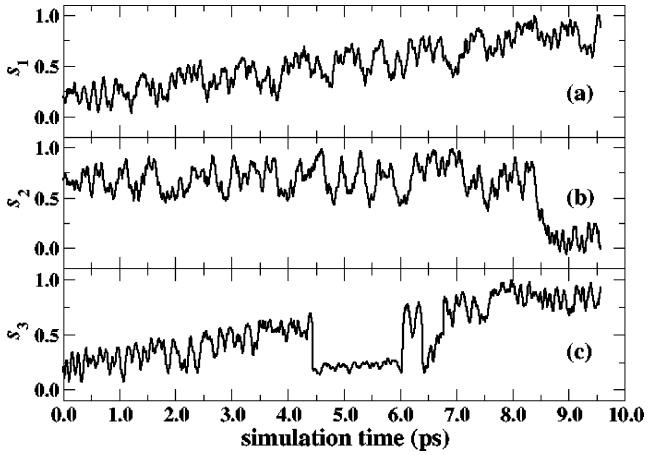

Figure 8. Evolution of the collective variables during the simulation for the case of an OH^- in the coordination shell of M_2. s_1, s_2, and s_3 are the coordination numbers of (a) P with $O^{2'}$, (b) P with $O^{5'}$, and (c) $O^{2'}$ with the nearby OH^- hydroxyl anion. Details are discussed in the text.

the vicinity of the catalytic site M_2. Furthermore, the presence of a hydroxyl anion has been shown to be essential in smoothing the Coulomb repulsion between the two Mg^{2+} ion catalysts when they are too close to each other.[67] In an attempt at understanding its detailed role, we repeated the metadynamics simulation with the two Mg^{2+} metal cations, substituting one of the water molecules in the solvation shell of M_2 with an OH^- (Figure 7, snapshot a). This particular choice is inferred by the known experimental data.[1,2,14,30,44,48] In this case, we assumed as collective variables s_1 and s_2 the coordination number between P and $O^{2'}$ [$s_1(t) = N_{coord}(P-O^{2'})$] and the coordination number between P and $O^{5'}$ [$s_2(t) = N_{coord}(P-O^{5'})$], as in the former simulation. For s_3, instead, we used the coordination number of the H atom of $-O^{2'}-H$ with the O atom of the hydroxyl anion [$s_3(t) = N_{coord}(H^{2'}-OH^-)$], since the detached proton is expected to form a water molecule with this OH^-. The fictitious effective masses were set to $M_1 = M_2 = 30$ au and $M_3 = 50$ au, and the harmonic coupling constants were $k_1 = k_2 = 0.6$ au and $k_3 = 0.8$ au for the three variables, respectively. A total simulation (meta)time of about 9.7 ps was required to explore the FES. The main steps of the reaction and the evolution of the collective variables are reported in Figures 7 and 8, respectively. In summary, between 4.4 and 6.5 ps, the proton of $O^{2'}-H$ jumps between the $O^{2'}$ oxygen and the OH^- group, being substantially a shared proton (Figure 7b), with M_2 playing its "usual" role in the $O^{2'}-H$ bond weakening. Eventually, at 6.7 ps (simulation time), the proton is stabilized on the OH^- anion that becomes a H_2O molecule, and the activation barrier for this process amounts to $\Delta E = 6.7 \pm 2.0$ kcal/mol and $\Delta F = 5.4 \pm 1.6$ kcal/mol for the total and free energies, respectively. This clearly indicates that, in the presence of a hydroxyl anion, this proton is released before the transition state and cannot be transferred to the ribozyme, in agreement with the experimental evidence,[44] and it is only after its release[2,45−48] that the nucleophilic attack of $O^{2'}$ to P can occur, leading to the formation of the TBP structure of Figure 7c. Furthermore, a noticeable decrease of the activation barrier characterizes the proton abstraction from the $-O^{2'}-H$ group if a metal ion and a hydroxyl anion are simultaneously present to cooperate. Once the OH^- is converted into a water molecule via the reaction $-O^{2'}-H + OH^- \rightarrow -O^{2'} + H_2O$, the role of M_2 is

terminated and the metal ion is free to migrate away from the ribozyme moiety keeping inside its solvation shell the newly formed H_2O molecule. Finally, when the evolution of $s_2(t)$ reaches a simulation (meta)time of 8.3 ps (Figure 7), the $P-O^{5'}$ bond undergoes a cleavage (Figure 7d), mediated by M_1, in a way similar to that of the previous cases. As soon as the bond is cleaved, a spontaneous water dissociation, $H_2O \rightarrow H^+ + OH^-$, occurs close to the departing group (Figure 7e), resulting in the protonation reaction $H_2O + R-O^{5'} \rightarrow R-O^{5'}-H + OH^-$. The OH^- anion is left behind, thus restoring the initial conditions, while the departing group, whose oxygen $O^{5'}$ is coordinated to M_1, moves away with the solvation shell of the metal ion. The overall activation barriers estimated are $\Delta E = 43.8 \pm 2.5$ kcal/mol and $\Delta F = 41.9 \pm 2.2$ kcal/mol for the total and free energies, respectively, and it must be remarked that they turn out to be the lowest among all the processes considered in the present work (Table 1). The lowering of the activation barrier can be ascribed to several factors. On one hand, the proton released by the $O^{2'}-H$ group is now significantly stabilized by its reaction with OH^- to form a H_2O molecule. On the other hand, the fact that this proton is not transferred to $O^{(S)}$, contrary to the case of the double-metal-ion reaction path discussed above, induces an intrinsic weakening of the $P-O^{5'}$ bond. This seems to be an important "preconditioning" factor that helps the subsequent bond cleavage.

3.4. The Role of an OH^- Hydroxyl Anion: Single-Metal-Ion Mechanism. Starting from an initial configuration pre-equilibrated for about 5 ps, reported in Figure 9a, a metadynamics simulation was performed in which the Mg^{2+} metal ion corresponding to the M_1 site was eliminated. The system obtained in this way is characterized by a local phosphate−metal−OH^- configuration that closely resembles the system studied in ref 30.

For this simulation, we adopted the same set of collective variables $\{s_1, s_2, s_3\}$ used in the former calculation with the same M_α and k_α ($\alpha = 1, 2, 3$) parameters, for the sake of consistency. The reaction path, in this case, is schematically summarized by the snapshots shown in Figure 9 from a to d. The presence of an OH^- in the solvation shell of the Mg^{2+} in the vicinity of $O^{2'}$ is again the triggering factor that promotes the proton abstraction (Figure 9b) and allows the subsequent nucleophilic attack of the phosphate. The TBP structure of panel c in Figure 9 represents the transition state and corresponds to the local maximum of the free energy surface along the metadynamics reaction path. In this simulation, at variance with the case of the double metal ion, we observed that the Mg^{2+} is still in the vicinity of the ribozyme system also at the end of the reaction (Figure 9 d) and keeps in its solvation shell $O^{2'}$.

The activation barriers were found to be $\Delta E = 51.6 \pm 2.9$ kcal/mol and $\Delta F = 49.2 \pm 2.7$ kcal/mol, thus, slightly lower (by about 5 kcal/mol) than in the case of the single-metal-ion reaction in the absence of OH^- (see Table 2). As in the former cases, the empty 3s orbital of Mg^{2+} overlaps the $O^{2'}$ atom, belonging to the solvation shell of the metal; this results in a weakening of the $O^{2'}-H$ bond and in an easier abstraction of the proton. Calculations on a similar model system have been reported in a recent work.[30]

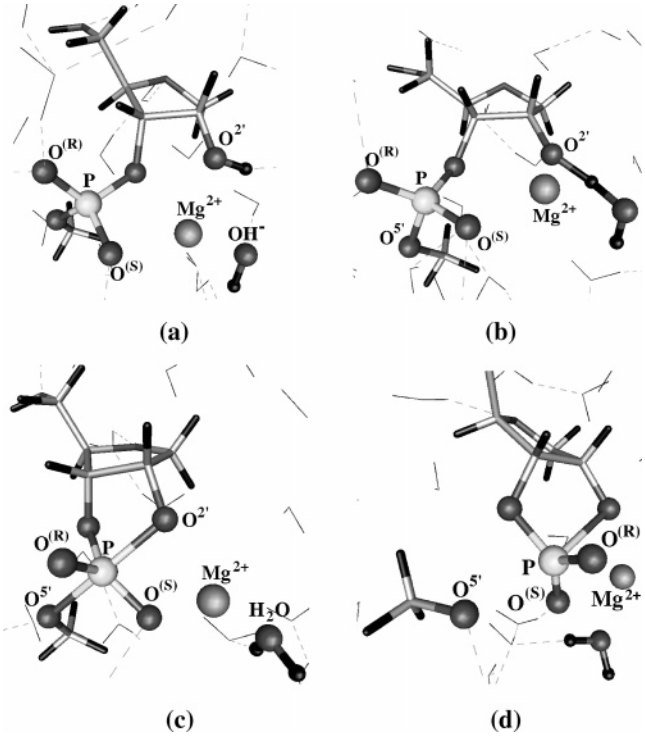

Figure 9. Initial configuration (a), proton abstraction from $O^{2'}$ (b), transition state (c), and final product (d) for the ribozyme system in the presence of a single Mg^{2+} metal ion and one OH^-. Surrounding H_2O molecules are shown as thin v-shaped sticks and H bonds as dashed light blue lines, and the most relevant atoms have been labeled for the sake of clarity.

However, a direct comparison is difficult since, there, static Gaussian calculations were performed, and apart from four H_2O molecules belonging to the solvation shell of the Mg^{2+}, the solvent is not explicitly accounted for in ref 30, but its effects are included by a conductor-like model. Thus, dynamical breaking and formation of H bonds with surrounding water molecules during the reaction are somehow missing. Nevertheless, the energy barriers estimated turn out to be 29.8 and 31.1 kcal/mol before empirical corrections for entropy and solvation effects. Similar results were recently obtained[68] by using a hybrid quantum mechanics/molecular mechanics approach. There, the authors adopt a semiempirical MNDO quantum approach with a CHARMM force field for the ribozyme model and a standard TIP3P model for the solvent water. However, no counterions are included, and this, along with the level of the quantum approach adopted, does not allow for figuring out a definitive picture. In both cases, these calculations seem to be closer to our double-metal-ion case and to the known experimental outcome.[1] As a matter of fact, the experiments are very difficult as well, and their results depend strongly on the environment, the type of ribozyme (hammerhead, hairpin, etc.), the metal cations' concentrations, and the (unknown) number of water molecules participating in the reaction.[1,2] Indeed, it is unclear if, in the ribozyme *pocket* in which the catalytic reaction occurs, the system is fully or only partially solvated. What can be inferred is that the cleavage activation energy can range roughly from 25 to 35 kcal/mol.

Since, as mentioned, the rate-limiting step of the reaction is the cleavage of the $P-O^{5'}$ bond, the computed activation

barriers are of, course higher, than the ones resulting from the double-metal-ion reaction. However, they are significantly lower than the analogous barriers computed for the single-metal-ion pathways in the absence of OH^-. This seems to support the notion that hydroxyl anions are a fundamental ingredient in the reaction mechanism and that at least one divalent metal cation is essential in catalyzing the reaction and enhancing the reaction rate. We observed that, along the whole reaction path, the metal ion does not coordinate directly to the *pro-R* $O^{(R)}$ atom. This is due to the fact that $O^{(R)}$ is, at each step, rather far from Mg^{2+} (∼4.20 Å in the initial configuration, ∼3.01 Å at the TBP, and ∼3.72 Å in the final state), and its approach to the metal cation would imply a very large distortion of the ribozyme model system. This result seems to be confirmed by the experimental evidence[69,70] and could provide support to the observed absence of thio effects in the hammerhead-ribozyme-mediated cleavage of a phosphorodithionate linkage.

4. Concluding Remarks

We have investigated, via first-principles dynamical simulations, the effects of metal cations in the cleavage reaction of RNA metalloenzymes. The simulations show that two metal catalysts play active roles in enhancing the reaction, and they play separately important roles in two different phases of the transesterification; thus, we can conclude that the major role of the metal ion at the M_1 site is to weaken the $P-O^{5'}$ bond. Conversely, the major contribution of the Mg^{2+} located at the M_2 site is to promote the release of H^+ from the $O^{2'}-H$ group. The absence of one of the two metals has been shown to lead to a distortion of the ribozyme structural model—that is not expected to occur in a more realistic, larger system—and to an increase in the activation barrier, thus lowering the reaction rate. This latter fact is due to the effects induced by divalent metal cations in withdrawing electronic charge from the chemical bonds that undergo a cleaving process. Thus, our analysis indicates rather clearly that a two-metal-ion mechanism is preferred with respect to a single-metal-ion one, leading to a remarkable enhancement of the reaction. Finally, we could shed some light on the proton-abstraction/proton-transfer mechanism from $O^{2'}-H$, underscoring the essential role played by a hydroxyl anion in the reaction, offering an interpretation of the experimental outcome. Finally, since the deprotonation of the $-O^{2'}-H$ group, although not being the rate-limiting step of the reaction, is an important aspect in the reaction pathway, the study presented here can provide a clue in understanding the role of metal ions in the proton-release process of several ribozymes and ribonucleases.[1,2,19−21]

Acknowledgment. We are grateful to Michele Parrinello, Alessandro Laio, Marcella Iannuzzi, Francesco L. Gervasio, Katsumasa Kamiya, and Takashi Ikeda for fruitful discussions. Calculations were performed on the computer facilities of Tsukuba University, ISSP—Tokyo University, and at the Computer Center for Agriculture, Foresty, and Fisheries Research (AFFRC) of the Japan Ministry of Agriculture, Foresty, and Fisheries. We acknowledge support from the Special Nanoscience Project—Tsukuba University and the ACT−JST program.

References

(1) Zhou, D.; Taira, K. *Chem. Rev.* **1998**, *98*, 991−1026.

(2) Perreault, D. M.; Anslyn, E. V. *Angew. Chem., Int. Ed. Engl.* **1997**, *36*, 432−450.

(3) Hutchins, C. J.; Rathjen, P. D.; Forster, A. C.; Symons, R. H. *Nucleic Acids Res.* **1986**, *14*, 3627−3640.

(4) Uhlenbeck, O. C. *Nature* **1987**, *328*, 596−600.

(5) Haseloff, J.; Gerlach, W. L. *Nature* **1988**, *334*, 585−591.

(6) Koizumi, M.; Iwai, S.; Otsuka, E. *Nucleic Acids Res.* **1989**, *17*, 7059−7071.

(7) Pley, H. W.; Flaherty, K. M.; McKay, D. B. *Nature* **1994**, *372*, 68−74.

(8) Murray, J. B.; Terwey, D. P.; Maloney, L.; Karpeisky, A.; Usman, N.; Biegelman, L.; Scott, W. G. *Cell* **1998**, *92*, 665−673.

(9) Buzayan, J. M.; Gerlach, W. L.; Bruening, G. *Nature* **1986**, *323*, 349−353.

(10) Santoro, S. W.; Joyce, G. F. *Proc. Natl. Acad. Sci. U.S.A.* **1997**, *94*, 4262−4266.

(11) Carola, C.; Eckstein, F. *Curr. Opin. Chem. Biol.* **1999**, *3*, 274−283.

(12) Bramlage, B.; Luzi, E.; Eckstein, F. *Trends Biotechnol.* **1998**, *16*, 434−438.

(13) Hermann, T.; Auffinger, P.; Westhof, E. *Eur. Biophys. J.* **1998**, *27*, 153−165.

(14) Fedor, M. J. *J. Mol. Biol.* **2000**, *297*, 269−291.

(15) Joyce, G. F. *Science* **2000**, *289*, 401−402.

(16) Schlutes, E. A.; Bartel, D. P. *Science* **2000**, *289*, 448−452.

(17) Yoshinari, K.; Taira, K. *Nucleic Acids Res.* **2000**, *28*, 1730−1742.

(18) Taira, K.; Nishikawa, S. In *Gene regulation: biology of antisense RNA and DNA*. Erickson, R. P., Izant, J. G., Eds.; Raven Press: New York, 1992; pp 35−54.

(19) Takagi, Y.; Warashina, M.; Stec, W. J.; Yoshinari, K.; Taira, K. *Nucleic Acids Res.* **2001**, *29*, 1815−1834.

(20) Oshima, K.; Kawasaki, H.; Soda, Y.; Tani, K.; Asano, S.; Taira, K. *Cancer Res.* **2003**, *63*, 6809−6814.

(21) Pyle, A. M. *Science* **1993**, *261*, 709−714.

(22) Steitz, T. A.; Steitz, J. A. *Proc. Natl. Acad. Sci. U.S.A.* **1993**, *90*, 6498−6502.

(23) Uchimaru, T.; Uebayashi, M.; Tanabe, K.; Taira, K. *FASEB J.* **1993**, *7*, 137−142.

(24) Scott, W. G.; Murray, J. B.; Arnold, J. R. P.; Stoddard, B. L.; Klug, A. *Science* **1996**, *274*, 2065−2069.

(25) Kuimelis, R. G.; McLaughlin, L. W. *Chem. Rev.* **1998**, *98*, 1027−1044.

(26) Zhou, D. M.; Taira, K. *Proc. Natl. Acad. Sci. USA* **1997**, *94*, 14343−14348.

(27) Zhou, J.; Zhou, D.; Takagi, Y.; Kasai, Y.; Inoue, A.; Baba, T.; Taira, K. *Nucleic Acids Res.* **2002**, *30*, 2374−2382.

(28) Li, Y.; Breaker, R. R. *J. Am. Chem. Soc.* **1999**, *121*, 5364−5372.

(29) Noodleman, L.; Lovell, T.; Han, W. G.; Li, J.; Himo, F. *Chem. Rev*. **2004**, *104*, 459−508.

(30) Torres, R. A.; Himo, F.; Bruice, T. C.; Noodleman, L.; Lovell, T. *J. Am. Chem. Soc*. **2003**, *125*, 9861−9867.

(31) Boero, M.; Terakura, K.; Tateno, M. *J. Am. Chem. Soc*. **2002**, *124*, 8949−8957.

(32) Zhang, B.; Cech, T. R. *Chem. Biol*. **1998**, *5*, 539−553.

(33) Kuwabara, T.; Warashima, M.; Taira, K. *Trends Biotechnol*. **2000**, *18*, 462−468.

(34) Uchimaru, T.; Tanabe, K.; Nishikawa, S.; Taira, K. *J. Am. Chem. Soc*. **1991**, *113*, 4351−4353.

(35) Dejaegere, A.; Lim, C.; Karplus, M. *J. Am. Chem. Soc*. **1991**, *113*, 4353−4355.

(36) Lim, C.; Karplus, M. *J. Am. Chem. Soc*. **1990**, *112*, 5872−5873.

(37) Storer, J. W.; Uchimaru, T.; Tanabe, K.; Uebayashi, M.; Nishikawa, S.; Taira, K. *J. Am. Chem. Soc*. **1991**, *113*, 5216−5219.

(38) Yliniemela, A.; Uchimaru, T.; Tanabe, K.; Taira, K. *J. Am. Chem. Soc*. **1993**, *115*, 3032−3033.

(39) Uchimaru, T.; Stec, W. J.; Tsuzuki, S.; Hirose, T.; Tanabe, K.; Taira, K. *Chem. Phys. Lett*. **1996**, *263*, 691−696.

(40) Doltsinis, N. L.; Sprik, M. *Phys. Chem. Chem. Phys*. **2003**, *5*, 2612−2618.

(41) Akola, J.; Jones, R. O. *J. Phys. Chem B* **2003**, *107*, 11774−11783.

(42) Alber, F.; Folkers, G.; Carloni, P. *THEOCHEM* **1999**, *489*, 237−245.

(43) Takagi, Y.; Taira, K. *J. Am. Chem. Soc*. **2002**, *124*, 3850−3852.

(44) Sawata, S.; Komiyama, M.; Taira, K. *J. Am. Chem. Soc*. **1995**, *117*, 2357−2358.

(45) Weinstein, L. B.; Jones, B. C.; Cosstick, R.; Cech, T. R. *Nature* **1997**, *388*, 805−808.

(46) Oivanen, M.; Kuusela, S.; Lönnberg, H. *Chem. Rev.* **1998**, *98*, 961−990.

(47) Lyne, P. D.; Karplus, M. *J. Am. Chem. Soc*. **2000**, *122*, 166−167.

(48) Dahm, S. C.; Derrick, W. B.; Uhlenbeck, O. C. *Biochemistry* **1993**, *32*, 13040−13045.

(49) Car, R.; Parrinello, M. *Phys. Rev. Lett*. **1985**, *55*, 2471−2474.

(50) CPMD code by J. Hutter et al. at MPI für Festkörperforschung and IBM Zurich Research Laboratory (1990−2004).

(51) Kohn, W.; Sham, L. J. *Phys. Rev. A: At., Mol., Opt. Phys.* **1965**, *140*, A1133−A1138.

(52) Hamprecht, F. A.; Cohen, A. J.; Tozer, D. J.; Handy, N. C. *J. Chem. Phys*. **1998**, *109*, 6264−6271.

(53) Boese, A. D.; Doltsinis, N. L.; Handy, N. C.; Sprik M. *J. Chem. Phys*. **2000**, *112*, 1670−1678.

(54) Troullier, N.; Martins, J. L. *Phys. Rev. B: Condens. Matter Mater. Phys.* **1991**, *43*, 1993−2006.

(55) Louie, S. G.; Froyen, F.; Cohen, M. L. *Phys. Rev. B: Condens. Matter Mater. Phys.* **1982**, *26*, 1738−1742.

(56) Nosé, S. *Mol. Phys*. **1984**, *52*, 255−268.

(57) Nosé, S. *J. Chem. Phys*. **1984**, *81*, 511−519.

(58) Hoover, W. G. *Phys. Rev. A: At., Mol. Opt. Phys.* **1985**, *31*, 1695−1697.

(59) Laio, A.; Parrinello, M. *Proc. Natl. Acad. Sci. U.S.A.* **2002**, *99*, 12562−12566.

(60) Iannuzzi, M.; Laio, A.; Parrinello, M. *Phys. Rev. Lett.* **2003**, *90*, 238302.

(61) Sprik, M.; Ciccotti, G. *J. Chem. Phys*. **1998**, *109*, 7737−7744.

(62) Segall, M. D.; Shah, R.; Pickard, C. J.; Payne, M. C. *Phys. Rev. B: Condens. Matter Mater. Phys.* **1996**, *54*, 16317−16320.

(63) Boero, M.; Ikeshoji, T.; Teralura, K.; Liew, C. C.; Parrinello, M. *J. Am. Chem. Soc*. **2004**, *126*, 6280−6286.

(64) Here and in every metadynamics simulation, the time has to be intended as the progress in the FES exploration and not as a "real" time, as explained in refs 59 and 60. Hence, it gives the energetically ordered sequence of the various steps of the reaction path along with the energy difference with respect to the initial potential well of the reactants.

(65) Because of the relatively large simulation cell, despite the periodic boundary conditions, on the time scale of the simulation, this OH^- does not recombine with the OH_3^+.

(66) In each case, the LUMO is a diffuse orbital, precursor state of a solvated electron. See, e.g., Boero, M.; Parrinello, M.; Terakura, K.; Ikeshoji, T.; Liew, C. C. *Phys. Rev. Lett*. **2003**, *90*, 226403.

(67) Hermann, T.; Auffinger, P.; Scott, W. G.; Westhof, E. *Nucleic Acids Res*. **1997**, *25*, 3421−3427.

(68) Gregersen, B. A.; Lopez, X.; York, D. M. *J. Am. Chem. Soc.* **2004**, *126*, 7504−7513.

(69) Warashima, M.; Takagi, Y.; Stec, W. J.; Taira, K. *Curr. Opin. Biotechnol*. **2000**, *11*, 354−362.

(70) Murray, J. B.; Scott, W. G. *J. Mol. Biol.* **2000**, *296*, 33−41.

CT050066Q